Single-molecule imaging of non-equilibrium molecular ensembles on the millisecond timescale

Manuel F. Juette[1,2], **Daniel S. Terry**[1,2], **Michael R. Wasserman**[1], **Roger B. Altman**[1], **Zhou Zhou**[1], **Hong Zhao**[1], and **Scott C. Blanchard**[1,3]

[1]Department of Physiology and Biophysics, Weill-Cornell Medical College, New York, NY, USA

Abstract

Molecular recognition is often driven by transient processes beyond the reach of detection. Single-molecule fluorescence microscopy methods are uniquely suited for detecting such non-accumulating intermediates, yet achieving the time resolution and statistics to realize this potential has proven challenging. Here, we present a single-molecule fluorescence resonance energy transfer (smFRET) imaging and analysis platform leveraging advances in scientific complementary metal-oxide semiconductor (sCMOS) detectors that enable the imaging of more than 10,000 individual molecules simultaneously at millisecond rates. The utility of this advance is demonstrated through quantitative measurements of previously obscured processes relevant to the fidelity mechanism in protein synthesis.

The potential of smFRET microscopy to capture transient, non-accumulating events at the level of individual molecules enables biological investigations unobscured by ensemble averaging[1, 2] and unconstrained by the need for large amounts of homogeneous material. The smFRET approach is based on detecting biological interactions from the perspective of motion, where a reaction coordinate is represented by changes in distance between individual particles or domains to which donor and acceptor fluorophores are site-specifically attached (Fig. 1a). While a growing number of biological systems have proven accessible to camera-based smFRET methods[2], cellular processes governed by micromolar affinity interactions[3, 4] and dynamics that occur on millisecond time scales[2, 5–8] are typically out of reach due to limited readout rates (Fig. 1b). Sub-millisecond time resolution can be achieved with avalanche photodiodes[9, 10], but only one molecule can be imaged at a time. Non-equilibrium processes can also be studied, but the time course of events must be

[3]Correspondence should be addressed to: S.C.B. (; Email: scb2005@med.cornell.edu)
[2]These authors contributed equally to this work.

inferred from snapshots recorded at precise lag times after microfluidic mixing[11, 12]. By contrast, camera-based methods simultaneously record the entire reaction coordinate in each molecule of the ensemble. Electron-multiplying charge-coupled device (EMCCD) cameras are well suited for single-molecule experiments, but are generally restricted to ~1,000 simultaneous observations at 10 ms time resolution. Reducing the EMCCD pixel array size[7, 13] offers increased imaging speeds, but at the expense of the number of observations (Fig. 1c), thereby defeating the goal of collecting sufficient statistics to fully characterize the ensemble.

Here we demonstrate a camera-based imaging platform that enables the acquisition of millisecond time scale steady-state and pre-steady-state smFRET measurements of over 10,000 individual molecules simultaneously (Fig. 1c). To achieve this goal, our strategy employs sCMOS detectors, rapid solution exchange (Fig. 1d), photostabilized fluorophores, and nearly real-time data analysis.

Commercially available sCMOS cameras have great potential for single-molecule imaging[14, 15], but their performance in smFRET applications has not yet been characterized. Our investigations demonstrate two key advantages of sCMOS for smFRET. First, sCMOS cameras have a higher effective quantum efficiency (QE) because signal multiplication by EMCCDs introduces excess noise that effectively halves QE[16]. Consequently, sCMOS yields superior signal-to-noise ratios (SNR) at signal levels of 200 or more detected photons per frame (Fig. 1e, **Online Methods**) and narrows FRET distributions by up to 25% (Fig. 1f). The advantage of EMCCD cameras extends only to photon counts below the typical prerequisite for accurately distinguishing FRET states[1, 2]. Second, sCMOS cameras have readout rates exceeding 400 megapixels per second, compared to just 30 for the fastest EMCCDs. This advantage provides marked increases in imaging throughput, exceeding one order of magnitude (Fig. 1c). Using one camera per spectral channel further increases throughput relative to commonly used split-camera optics[1] (Fig. 1d) to more than 10,000 molecules per movie at full frame.

At this scale of data generation, conventional analysis methods employing manual trace inspection and parameter tuning become prohibitively time consuming[17]. To address this challenge, we developed smFRET data analysis software optimized for sCMOS datasets (Fig. 1g, **Online Methods**, Supplementary Software 1). This pipeline provides automated tools for the analysis procedure, including: 1) identification of molecules in each spectral channel; 2) integration of pixel intensities into appropriately scaled and corrected, time-dependent fluorescence and FRET trajectories; 3) selection of desired fluorescence and FRET features according to user-defined criteria (Supplementary Table 1); 4) calculation of FRET observables (FRET value and state lifetimes) using hidden Markov modeling (HMM)[18, 19]; and 5) visualization of key experimental statistics for data interpretation. Minimizing the time and effort for such procedures facilitates real-time evaluations during data collection, empowering users with an objective approach to interpret and continue performing experiments effectively. Existing software packages[1, 18, 20_23], which require manual interventions and accommodate only a subset of these data analysis tasks, are incompatible with large sCMOS datasets.

As demonstrated by other high-throughput single-molecule platforms[24], large observation numbers enable stringent criteria to be applied to select long-lived FRET trajectories that exhibit functional heterogeneities or rare events that inform on the biological system. Imaging throughput is particularly critical for pre-steady-state, non-equilibrium smFRET measurements, such as single-turnover enzymatic reactions, in which the biological system evolves rapidly over time[7,25–28]. In contrast to steady-state observations, where data can be accumulated from multiple fields of view, the goal of pre-steady-state measurements is to acquire sufficient information on transient, non-accumulating events from the molecular ensemble in a single acquisition.

To evaluate the effectiveness of our imaging platform for pre-steady-state measurements, we investigated the process of transfer-RNA (tRNA) selection on the bacterial ribosome, a fidelity-determining step in protein synthesis that occurs at a bulk rate of approximately 10 s^{-1} *via* multiple short-lived intermediate states[7,25,29]. As previously established[7], tRNA selection can be visualized from the perspective of motion by tracking the evolution of smFRET as an acceptor-labeled aminoacyl-tRNA (aa-tRNA) – bound in a ternary complex (TC) with elongation factor Tu (EF-Tu) and GTP – enters a messenger RNA (mRNA)-programmed, surface-immobilized ribosome bearing a donor-labeled peptidyl-tRNA (Fig. 2a, **Online Methods**). Fidelity in the tRNA selection process entails a multi-step mechanism that preferentially allows cognate (correct) aa-tRNA to enter the ribosome to achieve a fully-accommodated, high-FRET state. Near- and non-cognate (incorrect) aa-tRNAs are rapidly and efficiently rejected at early stages in the selection process. At time resolutions necessary to detect intermediate states in tRNA selection, EMCCDs provide only a limited number of observations (typically < 50 events) in a single experiment (Supplementary Fig. 1a–b). By contrast, the sCMOS imaging platform provides datasets large enough (over 1,000 events) and of sufficient quality to quantitatively evaluate the kinetic behaviors of the ensemble from a single movie (Supplementary Fig. 1c–d). This increased throughput also enables comparisons of conditions and the examination of short-lived intermediates that are efficiently populated in the presence of protein synthesis inhibitors[30] (Supplementary Fig. 1e–n).

As expected from theoretical considerations[31], the initial phase of tRNA selection requires aa-tRNAs to be rapidly inspected by the ribosome as cognate aa-tRNAs represent only a small fraction of the cellular pool. This molecular recognition process takes place within a short-lived codon-recognition (CR) state that is poorly resolved at 10 ms time resolution[7], where over 60% of traces appear to skip the CR state. To better elucidate this initial selection step, we devised a distinct structural perspective wherein the CR state exhibits a high FRET efficiency that is more readily distinguished from background noise than the low-FRET CR state observed in the tRNA-tRNA system. Here, energy transfer occurs from a donor-labeled ribosomal protein (S12) to acceptor-labeled aa-tRNA entering the ribosome (Fig. 2b, **Online Methods**). The translation inhibitor tetracycline was added to promote rejection of aa-tRNA from the CR state, enabling detection of repeated, short-lived tRNA binding events at 1 ms time resolution (Fig. 2c) – more than 80% of which would have been missed at 10 ms (Fig. 2d). At this scale, anticipated distinctions in the lifetime of cognate and near-cognate mRNA codon-tRNA anticodon interactions were readily detected (Fig. 2e). These observations are

consistent with TC-ribosome interactions in the CR state being principally determined by codon-anticodon base-pairings, which are expected to fall in the high micromolar affinity regime with millisecond lifetimes[32, 33].

By employing pre-steady-state measurements (**Online Methods**), the complete tRNA selection process could be tracked from both structural perspectives (tRNA-tRNA and S12-tRNA) at 2 ms time resolution (Fig. 2f–h), such that intermediate states in the selection process were efficiently resolved, with over 86% of tRNA-tRNA FRET traces capturing CR dwells. This approach required rapid, reproducibly-timed injections of TC (Supplementary Fig. 2), as fast photobleaching in this imaging regime mandates precise synchronization of the start of the reaction with the beginning of illumination and data acquisition. As predicted from measurements and simulations of the tRNA selection process[7], short-lived, conformational sampling events of aa-tRNA within the aminoacyl (A) site were directly observed (Fig. 2f, h). The time-dependent ensemble progression to the accommodated states through intermediates could be directly followed on the single-molecule level (Fig. 2g). These experiments, which to our knowledge represent the highest time resolution camera-based pre-steady-state smFRET measurements reported to date, mark an important step toward single-molecule, rapid kinetics measurements of biological systems[4–7].

Our approach is readily applicable to a wide range of biological systems, especially those with overall rates indicative of intermediate states with millisecond residence times. This includes processive polymerization reactions (replication[26], transcription[27], reverse transcription[28]), protein folding[6], ATPase membrane transporters[34], and ion channels with millisecond activation-inactivation times[35].

The increased throughput of the platform may be particularly beneficial for multicolor non-equilibrium measurements, where relatively few particles may be correctly labeled or where the characteristically rapid photobleaching of blue/green and infrared fluorophores dominates. Complex, heterogeneous samples that cannot be obtained in large quantities, including intact viral particles[36] and mammalian systems[37], also stand to benefit from this platform.

Brighter, more photostable organic fluorophores will be critical to the pursuit of even faster time resolution measurements as the required illumination intensities tend to induce rapid photobleaching and pronounced blinking[2, 38]. Such advances will be paramount to increasing the velocity, breadth, and impact of single-molecule research and enabling investigations of molecular recognition processes with microsecond lifetimes and millimolar affinities.

Online Methods

Ribosome and reagent preparation

E. coli ribosomes, translation factors, fluorescently-labeled tRNAs, microfluidic chambers, buffers, and other reagents were prepared as previously described[7, 19, 25]. For tRNA-tRNA FRET experiments, ribosomes with ribosomal protein L1 deleted were used to reduce the appearance of hybrid states[19].

Preparation of S12-labeled ribosomes

Ribosomal protein S12 was PCR cloned from *E. coli* strain K12 genomic DNA into the pVB4 vector (Vectron Biosolutions) with an eight-residue peptide encoding the A4 epitope for the AcpS phosphopantetheinyl transferase reaction[39] (amino acid sequence: DSLDMLEW) fused at the C terminus. After plasmid shuffling into an *E. coli* S12 knockout strain[40], cells were cultured and ribosomes were harvested, cleaved and labeled with Cy3B *in situ* as performed previously for enzymatic labeling of S13-tagged subunits[41, 42]. To form intact 70S ribosome complexes, Cy3B-S12 30S and unlabeled BL21 (DE3) 50S subunits were heat activated at 42 °C for 10 min in Tris-polymix buffer containing 50 mM Tris-acetate pH 7.5, 5 mM $Mg(CH_3COO)_2$, 100 mM KCl, 5 mM $NH_4(CH_3COO)$, 0.5 mM $CaCl_2$, 0.1 mM EDTA, 5 mM putrescine, 1 mM spermidine, 1.5 mM β-mercaptoethanol, and 1 mM GTP. Ribosomes were then initiated with fMet-tRNA^{fMet} as previously described[25]. The assignment of FRET states for the S12 system (Fig. 2b) was validated using well-characterized translation inhibitors[43, 44] (Supplementary Fig. 3), similar to the approach used for previous assignments for the tRNA-tRNA signal[7].

Single-molecule fluorescence microscopy

Single-molecule FRET imaging of tRNA selection was performed using a custom prism-based total internal reflection fluorescence (TIRF) microscope as previously described[7, 25]. Ribosomes programmed with a biotinylated mRNA were surface immobilized to streptavidin, which was adhered to surface-linked biotin-polyethylene glycol. The mRNA codon in the ribosomal A site was either cognate (UUC) or near-cognate (UCU) to the tRNA^{Phe} anticodon (AAG). All experiments were performed in Tris-polymix buffer (see above) in the presence of an oxygen scavenging system (2 mM protocatechuic acid, 50 nM protocatechuate 3,4-dioxygenase)[45] and photostabilizing agents (1 mM Trolox, 2 mM cyclooctatetraene, 1 mM nitrobenzyl-alcohol)[46].

Cy3 fluorophores (Cy3 or Cy3B) on P-site tRNA or S12 were illuminated with a 532 nm diode-pumped solid state laser (Opus, LaserQuantum) at ~0.45 to 2 kW/cm^2 (at the TIR interface) for time resolutions between 10 ms and 1 ms. An area larger than the imaging field of view was illuminated to optimize uniformity by appropriate placement of the $f = 150$ mm focusing lens relative to the TIR prism. Additionally, a telescopic arrangement of cylindrical lenses ($f_1 = -50$ mm and $f_2 = 100$ mm) was placed in the excitation beam path to correct for the non-uniform projected beam aspect ratio at the TIR interface. It is also worth noting that any poorly illuminated or aberrant molecules in the corners of the field of view can be removed using the automated analysis procedure and that the large datasets obtainable with sCMOS ensure that the resulting subsets are large enough to determine the parameters of interest. An ET555lp long pass filter (Chroma) was used to remove scattered laser light. Fluorescence emission from Cy3 (or Cy3B) and LD650 (Lumidyne Technologies)[47] fluorophores was collected using a 60 ×, 1.27 N.A. PlanApo water immersion objective (Nikon), spectrally separated using a MultiCam-LS device (Cairn) using a T635lpxr-UF2 dichroic mirror (Chroma) and imaged onto two Hamamatsu ORCA-Flash 4.0 v2 sCMOS cameras (2,084 × 2,048 pixels, 6.5 μm pixel size) connected to a PC with Camera Link acquisition boards. The instrument was also equipped with additional laser lines (Ciel 473 nm, LaserQuantum; Genesis MX 639 nm, Coherent; 730 nm collimated

diode, Leading-Tech Laser), two additional cameras (connected to the same MultiCam-LS device) and dichroic mirrors (ZT532rdc-UF2, T740lpxr-UF2) for additional spectral channels in the Cy2 and Cy7 regions.

Data were acquired using custom software implemented in LabView (National Instruments). 2×2 pixel binning (217 nm effective pixel size in the sample plane accounting for magnification) was chosen to minimize the data size without sacrificing any measure of data quality. A pixel size satisfying the Nyquist sampling criterion is not required to measure the total intensity of each diffraction-limited molecule image, but excessive binning decreases the resolvable molecule density. In contrast to EMCCD cameras, binning on an sCMOS sensor does not increase the achievable frame rate. The total field of view was 222 μm × 222 μm in the sample plane at 10 ms time resolution. Synchronization of the cameras was achieved with an external pulse to trigger the acquisition of each frame. The pulse sequence was generated in real time by a USB device (USB-6501, National Instruments) controlled by the acquisition software. The timing and reproducibility of this approach was verified both by examining oscilloscope outputs and by testing the synchronization of camera frames with an external light source. Movies were streamed to a solid state drive during acquisition using the built-in HD recorder of the Hamamatsu camera driver. The generated raw data files were tiled side by side and automatically converted to the BigTIFF format, a proposed standard for image files exceeding 4 GB in size (http://www.awaresystems.be/imaging/tiff/bigtiff.html), using a custom library implemented in C (Supplementary Software 2). New movie files were automatically detected and processed as described under *Particle detection and generation of fluorescence traces* below, ready for immediate inspection by the user.

For EMCCD measurements of tRNA selection, a DualCam device (Photometrics) using a 640dclp dichroic mirror (Chroma) was used to spectrally separate Cy3 and LD650 fluorescence and image the molecules onto two Evolve 512 cameras (Photometrics) with 512×512 pixels and 16 μm physical pixel size. Data were acquired in MetaMorph (Molecular Devices) with the 10 MHz chipset and 2×2 pixel binning (533 nm effective pixel size), chosen to balance throughput and data quality. Synchronization was achieved by triggering each frame with a custom timing circuit. A rectangular region of interest (137 μm × 68 μm in the sample) covering the bottom half of the field of view was used to achieve 10 ms imaging (Fig. 1c). For direct quantitative comparisons of sCMOS and EMCCD measurements, the two pairs of cameras were attached to the same two output ports of the MultiCam device and integration regions (see below) chosen to account for the difference in effective pixel size of the two camera models. Comparative measurements were performed using DNA standards labeled with LD550 and LD650 fluorophores (Lumidyne Technologies) following previously established protocols[48]. SNR and FRET distribution statistics (Fig. 1e–f) were computed as described below.

Fast (1–2 ms) tRNA selection experiments

A rectangular region of interest consisting of 200 (400) lines at the center of the field of view was used to achieve 1 ms (2 ms) imaging (Fig. 1c), corresponding to 222 μm × 22 μm (222 μm × 43 μm) field of view in the sample. Multiple movies were combined for each condition. Measurements at 1 ms time resolution were performed in the presence of 20 μM

tetracycline (Fig. 2c,e) or with TC containing the non-hydrolysable GTP analog GDPNP (Fig. 2d) to terminate selection events prior to completion of the initial selection phase. To verify that the resulting short FRET events represent specific interactions, control experiments were performed with Cy5-labeled DNA oligonucleotides instead of TC, showing low numbers of non-specific or misidentified events (41.5 vs. 4.8 on average per movie, respectively). The lifetimes of CR interactions (Fig. 2e) were determined by fitting a sum of two exponentials, $a\,e^{-k_1 t} + (1 - a)e^{-k_2 t}$, to the survival plot and calculating the lifetime τ as the inverse of the amplitude-weighted average of the rates k_1 and k_2. The results with 95 % confidence intervals were as follows: cognate – $a = 0.687 \pm 0.025$, $k_1 = 0.293 \pm 0.012$ ms^{-1}, $k_2 = 0.058 \pm 0.004$ ms^{-1}; near-cognate – $a = 0.967 \pm 0.035$, $k_1 = 0.459 \pm 0.035$ ms^{-1}, $k_2 = 0.043 \pm 0.057$ ms^{-1}.

To achieve reproducible timing for pre-steady-state experiments, TC was prepared at the final concentration in oxygen-scavenging buffer and loaded into a pressure-resistant steel syringe (Harvard Apparatus), which was then attached to a syringe pump (PHD Ultra, Harvard Apparatus). Reagent delivery from the pump to the microfluidic devices was triggered by the custom acquisition software to ensure reproducibility to within 2 ms (Supplementary Fig. 2). The synchronization of the ensemble process is limited by reproducibility and rise time of reagent delivery (inherent properties of the instrument), and the stochastic arrival time distribution determined by the bimolecular rate constant of the interaction. It should be noted, however, that one of the strengths of single-molecule experiments is that this asynchrony can be eliminated by synchronizing individual traces to the point of the first registered FRET transition as described below. The purpose of hardware synchronization is mainly to ensure that mixing is complete prior to photobleaching so that the full process can be observed.

Particle detection and generation of fluorescence traces

smFRET data analysis[1, 17] was performed using custom software written in MATLAB (Supplementary Software 1). The process begins with the detection of fluorophore-labeled particles, which appear as local intensity maxima (point-spread functions, PSFs) above baseline levels in fixed positions within the field-of-view[49] (Fig. 1g, left panel). Since they are fixed, particles are detected from an average image of the first 10 frames of the movie[1]. Prior to detection, a background image is subtracted to flatten baseline levels and ease molecule detection, particularly when the illumination is nonuniform. The background image is generated by dividing the field into a grid, taking an average of the 5% lowest intensity pixels in each grid area, and interpolating these values to generate a full-field image, similar to other methods[1, 50]. Intensity maxima associated with fluorophore-labeled particles are distinguished from background using a threshold of eight s.d. above background noise. Any molecules that are stochastically closer than three average PSF s.d. apart are rejected to avoid signal contamination between neighboring particles.

Next, intensity maxima in each spectral channel corresponding to the same particle are associated using the iterative closest point (ICP) algorithm[51, 52], resulting in a transformation that accounts for translation, rotation, and magnification. The algorithm is robust to large alignment deviations, particles without a signal in all spectral channels, and

background fluorescence. The procedure is automated and does not require the user to select control points[1]. In difficult cases where one channel has low signal, the alignment transformation can instead be derived using fluorescent beads prior to the experiment. Robust software alignment is critical to the success of sCMOS imaging because its larger field of view and higher pixel density result in larger deviations in pixel units compared to EMCCDs.

After image registration using the transformation derived above, particles are re-detected from a summed image of all spectral channels[1] to minimize any potential selection bias. For example, particles with a low FRET efficiency may not have sufficient intensity on the acceptor channel to be detected, so the remaining population would be biased towards particles with higher FRET efficiency. When the intensities from all spectral channels are summed, particles will have roughly the same overall intensity regardless of FRET efficiency.

Finally, fluorescence-time traces for each particle are extracted from the movie by summing the intensity of the highest intensity pixels within a small neighborhood around the maximum[50]. The neighborhood size is chosen to be five times the average PSF s.d. The optimal number of pixels balances the trade-off between collecting more fluorescence intensity and also collecting more background noise, but only needs to be determined once for a particular instrument. This is similar to aperture photometry[1,22,23] in that it is computationally simple and fast, while PSF fitting is relatively slow even with extensive optimization. While PSF fitting[22,23] has potential advantages to handle non-uniform PSFs, uneven focus, stage or focal drift, and noise characteristics of the detector[15], in our experience it does not significantly improve data quality obtained with a stable, well-corrected instrument.

Baseline subtraction, spectral corrections, and FRET calculation

In order to interpret FRET efficiency as a measure of the distance between donor and acceptor fluorophores, several experimental considerations must be taken into account: fluorescence baseline, spectral crosstalk, and the apparent sensitivity for each fluorophore (schematized in Fig. 1g, second panel from the left). First, the baseline intensity levels after donor photobleaching are subtracted from fluorescence traces to set the baseline level close to zero, refining the earlier estimate obtained by subtracting an approximate background image. The donor photobleaching point is detected as the last large drop in the gradient of median-filtered total fluorescence intensity (six s.d. beyond the noise). While aperture photometry[1,22,23] has the advantage of adjusting for changing baseline levels, it also requires a large clear area around each PSF, limiting the density of particles that can be imaged simultaneously.

Next, the fraction of donor fluorescence appearing on the acceptor channel (spectral crosstalk, a), estimated from the acceptor channel intensity after acceptor photobleaching, is subtracted from acceptor fluorescence traces so that the apparent crosstalk is zero. To ensure the relative brightness of the fluorophores is equal, the change in donor and acceptor fluorescence upon acceptor photobleaching is used to estimate the relative brightness (γ)[1,50] and the average value is used to scale the acceptor intensity. In both cases, a single, average

correction value is used for all traces in each movie because the imperfect estimates in each trace can add variability, rather than reducing it.

Finally, FRET-time traces are calculated as $E_{FRET} = I_A/(I_A + I_D)$, where I_A and I_D are the acceptor and donor fluorescence intensity at each point in time, respectively. FRET is set to zero after donor photobleaching and during donor blinking events, which are detected whenever total intensity drops below six standard deviations of background noise. The high noise levels and non-ideal photophysical behavior apparent in millisecond smFRET data necessitate an alternative strategy that is more robust to noise: the total fluorescence intensity trace $(I_A + I_D)$ is idealized with a two-state model for fluorescent and dark states using the segmental K-means algorithm (SKM)[53] implemented in MATLAB.

Calculation of trace statistics and trace selection

Automated trace selection is achieved by calculating a set of statistics for each trace and choosing a useful subset according to defined criteria (Fig. 1g, third panel from the left). Commonly used statistics, selection criteria, and the purpose of each are listed in Supplementary Table 1.

Signal-to-noise ratio (SNR) is a measure of trace quality, which ultimately determines the capability to distinguish distinct FRET states. SNR_{BG} is defined as the mean total fluorescence intensity (MTI) divided by the standard deviation of background total intensity immediately after donor photobleaching (100 frames). A distinct "background noise" statistic defines the s.d. of the entire trace after photobleaching, which is useful for detecting unstable background levels. SNR_{Signal} is defined as the MTI divided by the standard deviation of total intensity before donor photobleaching, ignoring regions where the donor is dark. This metric more closely corresponds to the noise in the measurement since it takes into account photon statistics and photophysical noise.

For detecting traces with an acceptor signal above baseline, a threshold of 0.125 FRET is used, corresponding to two standard deviations above typical background noise levels[7, 19]. "FRET lifetime" is a statistic that quantifies the observation time for FRET, where the acceptor signal is above background, primarily for experiments where the acceptor fluorophore is stably bound. To reduce false positives from traces that happen to have high background noise, only runs of five frames or more above the threshold are considered.

Single-molecule traces are generally only useful if they contain exactly one donor and one acceptor signal. The number of donor fluorophores can be determined by counting the number of photobleaching steps, which appear as instantaneous, irreversible drops in the total fluorescence intensity (donor + acceptor). Detection is accomplished by median filtering the signal with a window size of nine frames to remove high frequency noise, while preserving sharp changes, and taking the gradient to detect the large, sudden drops in fluorescence intensity associated with photobleaching steps. A threshold of four standard deviations of the gradient signal is used for detecting these events. A photobleaching event is counted if the intensity never returns to the level before the event.

Bias in these parameters is estimated by comparing the population behavior of a selected subset of data to the full dataset. This procedure should be repeated for any new biological sample or type of experiment to ensure that selection is unbiased.

Hidden Markov modeling

FRET events, corresponding to tRNA binding to the ribosome, are isolated and post-synchronized as previously described[7]. State assignment (Fig. 1g, right panel) is performed using SKM[53]. Although several other Markov modeling utilities are available and could be used for this purpose (HaMMy[18], vbFRET[20], SMART[21], iSMS[22], TwoTone[23]), SKM is much faster[17] and this facilitates analysis of the large datasets associated with sCMOS.

Code availability

Source code for the data analysis software is freely available. Contact scb2005@med.cornell.edu for more information.

Supplementary Material

Refer to Web version on PubMed Central for supplementary material.

Acknowledgments

References

1. Roy R, Hohng S, Ha T. Nat Methods. 2008; 5:507–516. [PubMed: 18511918]

2. Juette MF, et al. Curr Opin Chem Biol. 2014; 20:103–111. [PubMed: 24956235]

3. Cisse, Kim H, Ha T. Nat Struct Mol Biol. 2012; 19:623–627. [PubMed: 22580558]

4. Gromadski KB, Wieden HJ, Rodnina MV. Biochemistry. 2002; 41:162–169. [PubMed: 11772013]

5. Henzler-Wildman K, Kern D. Nature. 2007; 450:964–972. [PubMed: 18075575]

6. Chung HS, McHale K, Louis JM, Eaton WA. Science. 2012; 335:981–984. [PubMed: 22363011]

7. Geggier P, et al. J Mol Biol. 2010; 399:576–595. [PubMed: 20434456]

8. Juette MF, Bewersdorf J. Nano Lett. 2010; 10:4657–4663. [PubMed: 20939601]

9. Chung HS, Gopich IV. Phys Chem Chem Phys. 2014; 16:18644–18657. [PubMed: 25088495]

10. Ha T, Chemla DS, Enderle T, Weiss S. Appl Phys Lett. 1997; 70:782–784.

11. Wunderlich B, et al. Nat Protoc. 2013; 8:1459–1474. [PubMed: 23845960]

12. Gambin Y, et al. Nat Methods. 2011; 8:239–241. [PubMed: 21297620]

13. Kim E, et al. Nat Chem Biol. 2013; 9:313–318. [PubMed: 23502425]

14. Saurabh S, Maji S, Bruchez MP. Opt Express. 2012; 20:7338–7349. [PubMed: 22453414]

15. Huang F, et al. Nat Methods. 2013; 10:653–658. [PubMed: 23708387]

16. Pawley, JB. Handbook Of Biological Confocal Microscopy. 3. Pawley, JB., editor. Springer; US, New York, NY, USA: 2006. p. 918-931.

17. Blanco M, Walter NG. Methods Enzymol. 2010; 472:153–178. [PubMed: 20580964]

18. McKinney SA, Joo C, Ha T. Biophys J. 2006; 91:1941–1951. [PubMed: 16766620]

19. Munro JB, Altman RB, O'Connor N, Blanchard SC. Mol Cell. 2007; 25:505–517. [PubMed: 17317624]

20. Bronson JE, Fei J, Hofman JM, Gonzalez RL Jr, Wiggins CH. Biophys J. 2009; 97:3196–3205. [PubMed: 20006957]

21. Greenfeld M, Pavlichin DS, Mabuchi H, Herschlag D. PLoS One. 2012; 7:e30024. [PubMed: 22363412]

22. Preus S, Noer SL, Hildebrandt LL, Gudnason D, Birkedal V. Nat Methods. 2015; 12:593–594. [PubMed: 26125588]

23. Holden SJ, et al. Biophys J. 2010; 99:3102–3111. [PubMed: 21044609]

24. Chen J, et al. Proc Natl Acad Sci USA. 2014; 111:664–669. [PubMed: 24379388]

25. Blanchard SC, Gonzalez RL, Kim HD, Chu S, Puglisi JD. Nat Struct Mol Biol. 2004; 11:1008–1014. [PubMed: 15448679]

26. Lee SJ, et al. Proc Natl Acad Sci USA. 2014; 111:E827–E835. [PubMed: 24550505]

27. Duzdevich D, Redding S, Greene EC. Chem Rev. 2014; 114:3072–3086. [PubMed: 24400809]

28. Abbondanzieri EA, et al. Nature. 2008; 453:184–189. [PubMed: 18464735]

29. Rodnina MV, Wintermeyer W. Annu Rev Biochem. 2001; 70:415–435. [PubMed: 11395413]

30. Polikanov YS, et al. Mol Cell. 2015; 58:832–844. [PubMed: 26028538]

31. Johansson M, Lovmar M, Ehrenberg M. Curr Opin Microbiol. 2008; 11:141–147. [PubMed: 18400551]

32. Labuda D, Striker G, Grosjean H, Porschke D. Nucleic Acids Res. 1985; 13:3667–3683. [PubMed: 4011439]

33. Guéron, M.; Leroy, J-L. Nucleic Acids and Molecular Biology. Eckstein, F.; Lilley, DMJ., editors. Springer; Berlin, Heidelberg: 1992. p. 1-22.

34. Moller JV, Olesen C, Winther AM, Nissen P. Q Rev Biophys. 2010; 43:501–566. [PubMed: 20809990]

35. Armstrong CM. Annual Review of Physiology. 2007; 69:1–18.

36. Munro JB, et al. Science. 2014

37. Ferguson A, et al. Molecular Cell. 2015; 60:475–486. [PubMed: 26593721]

38. Zheng Q, et al. Chem Soc Rev. 2014; 43:1044–1056. [PubMed: 24177677]

39. Zhou Z, Koglin A, Wang Y, McMahon AP, Walsh CT. J Am Chem Soc. 2008; 130:9925–9930. [PubMed: 18593165]

40. Shoji S, Dambacher CM, Shajani Z, Williamson JR, Schultz PG. J Mol Biol. 2011; 413:751–761. [PubMed: 21945294]

41. Wang L, et al. Nat Struct Mol Biol. 2012; 19:957–963. [PubMed: 22902368]

42. Wasserman MR, et al. Nat Commun. 2015; 6:7896. [PubMed: 26224058]

43. Jenner L, et al. Proc Natl Acad Sci USA. 2013; 110:3812–3816. [PubMed: 23431179]

44. Schuette JC, et al. EMBO J. 2009

45. Aitken CE, Marshall RA, Puglisi JD. Biophys J. 2008; 94:1826–1835. [PubMed: 17921203]

46. Dave R, Terry DS, Munro JB, Blanchard SC. Biophys J. 2009; 96:2371–2381. [PubMed: 19289062]

47. Akyuz N, et al. Nature. 2015; 518:68–73. [PubMed: 25652997]

48. Altman RB, et al. Nat Methods. 2012; 9:68–71. [PubMed: 22081126]

49. Ha T, et al. Proc Natl Acad Sci U S A. 1999; 96:893–898. [PubMed: 9927664]

50. McCann JJ, Choi UB, Zheng L, Weninger K, Bowen ME. Biophys J. 2010; 99:961–970. [PubMed: 20682275]

51. Chen Y, Medioni G. IEEE Int Conf Robot. 1991:2724–2729.

52. Besl PJ, Mckay ND. Ieee T Pattern Anal. 1992; 14:239–256.

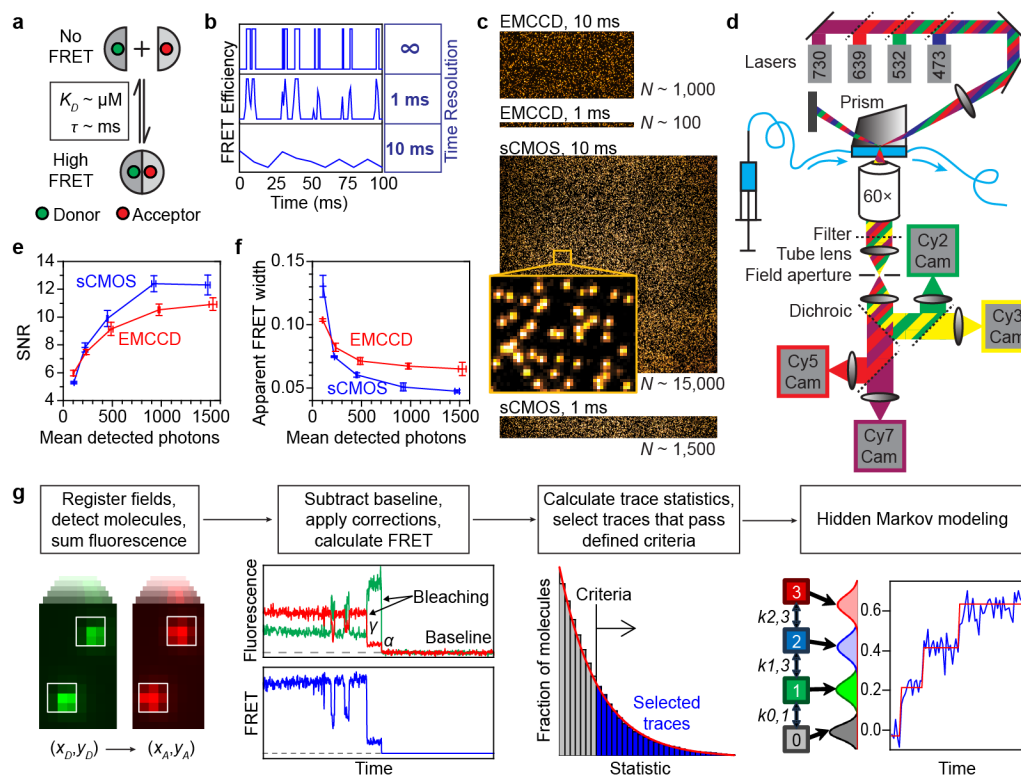53. Qin F. Methods Mol Biol. 2007; 403:253–286. [PubMed: 18828000]

Figure 1.

Imaging platform for enhanced-throughput smFRET. (**a**) Schematic of a molecular interaction monitored by FRET (K_D – dissociation constant; τ – interaction lifetime). (**b**) FRET signal for **a**, modeled at infinite time resolution (top) and downsampled to 1 and 10 ms (middle/bottom), highlighting how insufficient sampling hinders the detection of events. (**c**) Comparison of fields of view and numbers of molecules observed (N) with typical EMCCD and sCMOS cameras at 1 and 10 ms time resolution. (**d**) Schematic of the experimental setup with prism-type TIR excitation, fluorescence detection *via* a $60 \times$ water-immersion objective, one sCMOS camera per spectral channel, and microfluidic reagent delivery system. Comparison of (**e**) average SNR and (**f**) width of the observed FRET distribution of data obtained from a dye-labeled DNA duplex standard at various intensity levels (sCMOS in blue, EMCCD in red; center/error bars: mean/s.d. of four technical replicates). (**g**) Schematic of automated data analysis pipeline. Left to right: molecules are detected and aligned in each spectral channel and their signals summed to create fluorescence-time traces; corrections are made for baseline, spectral bleed-through (α) and unequal apparent brightness (γ) and FRET-time traces (blue) are calculated; descriptive statistics are calculated for each trace (distribution in bars) and traces are selected that pass user-defined fitness criteria (blue bars); Hidden Markov modeling (HMM) with a kinetic (left) and emission (middle) model is used to interpret the dynamic behavior in FRET traces (right) and assign the underlying physical state of the system at each point in time (idealization, red line).
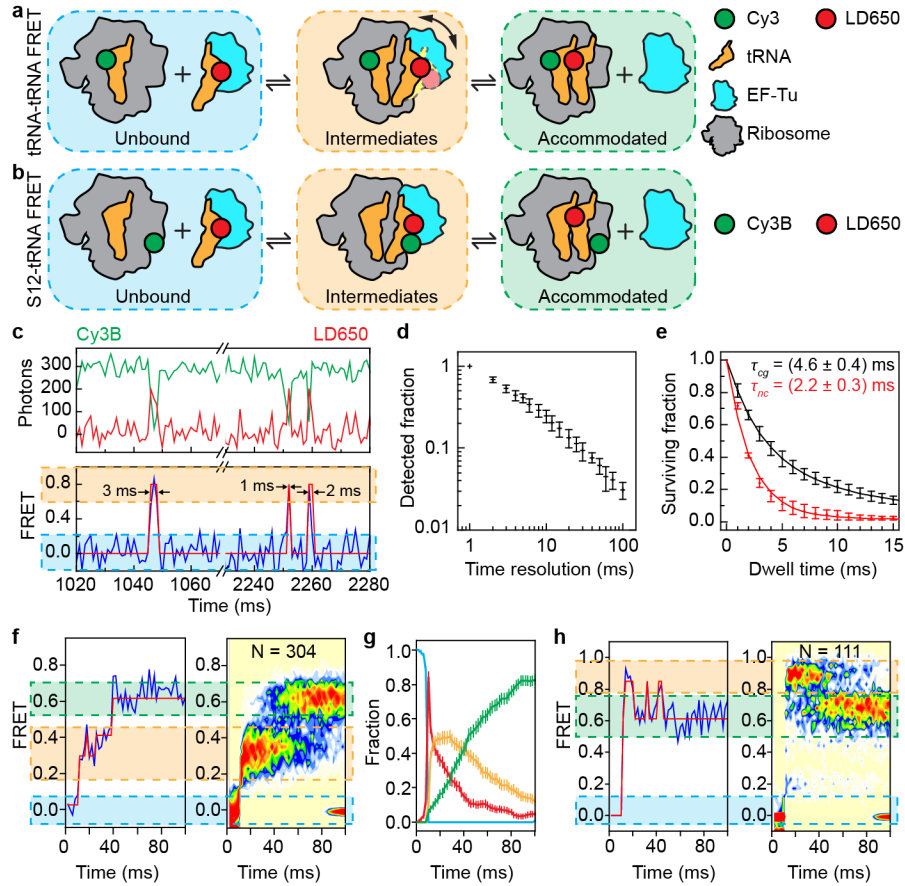
Figure 2.
Robust detection of millisecond-scale transient events by smFRET. (**a**) Schematic of the tRNA-tRNA FRET experiment. TC is delivered to surface-immobilized ribosomes (no FRET, blue) containing a cognate mRNA codon in the A site. Accommodation (high-FRET, green) occurs via short-lived intermediates (mid-FRET, orange). (**b**) Equivalent schematic of the S12-tRNA FRET experiment. Here, intermediates correspond to high-FRET, accommodation to mid-FRET. (**c**) Fluorescence (top) and FRET (bottom) time traces of a single ribosome displaying short-lived TC binding events in the presence of the tRNA selection inhibitor tetracycline (20 μM concentration). The idealized FRET trace is shown in red. (**d**) Fraction of binding events that are detected as a function of time resolution, obtained by downsampling 1 ms data and normalizing to the number of events observed at 1 ms. Centers/error bars: mean/s.d. of three technical replicates. (**e**) Exponential fits (lines) to the survival time in the high-FRET state reveal lifetimes of 4.6 ms for the cognate (τ_{cg} – black) and 2.2 ms for a near-cognate codon-anticodon interaction (τ_{nc} – red). Centers/error bars: mean/s.d. of three technical replicates. (**f**–**h**) Pre-steady-state tRNA selection experiments (2 ms time resolution) comparing the tRNA-tRNA (**f**–**g**) and S12-tRNA (**h**) signals. (**f, h**) left panels: example FRET traces; right panels: post-synchronized ensemble plots; (**g**) occupancy of each FRET state as a function of time (blue line – no FRET/ unbound, red line – low FRET/codon recognition, orange line – mid FRET/GTPase

activation, green line – high FRET/accommodated). Error bars: s.e. from 1,000 bootstrap samples.